Environmental Pollution 298 (2022) 118857

Contents lists available at ScienceDirect

Environmental Pollution

journal homepage: www.elsevier.com/locate/envpol

Raman imaging of microplastics and nanoplastics generated by cutting PVC pipe☆

Yunlong Luo [a,b], Md Al Amin [a], Christopher T. Gibson [c,d], Clarence Chuah [d], Youhong Tang [d], Ravi Naidu [a,b], Cheng Fang [a,b,*]

[a] Global Centre for Environmental Remediation (GCER), University of Newcastle, Callaghan, NSW, 2308, Australia
[b] Cooperative Research Centre for Contamination Assessment and Remediation of the Environment (CRC CARE), University of Newcastle, Callaghan, NSW, 2308, Australia
[c] Flinders Institute for NanoScale Science and Technology, College of Science and Engineering, Flinders University, South Australia, 5042, Australia
[d] Flinders Microscopy and Microanalysis, College of Science and Engineering, Flinders University, Bedford Park, 5042, Australia

ARTICLE INFO

Keywords:
Raman imaging
Microplastics
Nanoplastics
PVC pipe
Logic-based algorithm

ABSTRACT

The characterisation of nanoplastics is much more difficult than that of microplastics. Herewith we employ Raman imaging to capture and visualise nanoplastics and microplastics, due to the increased signal-noise ratio from Raman spectrum matrix when compared with that from a single spectrum. The images mapping multiple characteristic peaks can be merged into one using logic-based algorithm, in order to cross-check these images and to further increase the signal-noise ratio. We demonstrate how to capture and identify microplastics, and then zoom down gradually to visualise nanoplastics, in order to avoid the shielding effect of the microplastics to shadow and obscure the nanoplastics. We also carefully compare the advantages and disadvantages of Raman imaging, while giving recommendations for improvement. We validate our approach to capture the microplastics and nanoplastics as particles released when we cut and assemble PVC pipes in our garden. We estimate that, during a cutting process of the PVC pipe, thousands of microplastics in the range of 0.1–5 mm can be released, along with millions of small microplastics in the range of 1–100 μm, and billions of nanoplastics in the range of <1 μm. Overall, Raman imaging can effectively capture microplastics and nanoplastics.

1. Introduction

Plastics are unquestionably some of the most versatile materials in modern life. Plastic items are generally lightweight and durable, but they come with a significant environmental cost (Petersen and Hubbart, 2021). Plastic waste can come in all shapes and sizes, and plastic particles, fragments and fibres <5 mm in diameter or length are referred to as microplastics. Previous research has underlined the pervasive spread of microplastics into virtually every crevice on earth, infiltrating both poles (Barnes et al., 2010; Ross et al., 2021), Mount Everest (Napper et al., 2020) and the deepest point of the ocean (Jamieson et al., 2017). While microplastics have caused significant concerns, nanoplastics of <1 μm might be more serious in terms of toxicity and abundance (Buranyi, 2020; Gigault et al., 2021; Li et al., 2020; Sun et al., 2020). Unfortunately, the research on nanoplastics is far behind the research on microplastics. Perhaps the main reason is due to the characterisation of nanoplastics, which is much more difficult than that of microplastics, and currently no effective approach is available. Consequently, little is known about the nanoplastics with regards to their source, fate, risk etc. (Gigault et al., 2021).

PVC is an inexpensive, readily available, and highly rigid plastic material that shows considerable physical and chemical resistance (Kaczorek-Chrobak and Fangrat, 2020; William Coaker, 2003). Being widely used, and if being wrongly disposed, PVC is deemed to be one of the most hazardous plastics with severe health risks and environmental impacts, due to the potential release of harmful additives, such as phthalates, bisphenol A, dioxin, lead and cadmium during its life cycle (Proshad et al., 2018). The leaching process tends to be accelerated after the fragmentation of plastics into microplastics and nanoplastics that feature extremely high specific surface area (Boyle et al., 2020; Naik et al., 2020). For example, PVC pipes often need to be cut into the right size to meet specific purposes and microplastics are possibly produced,

☆ This paper has been recommended for acceptance by Eddy Y. Zeng

* Corresponding author. Global Centre for Environmental Remediation (GCER), University of Newcastle, Callaghan, NSW, 2308, Australia.
E-mail address: cheng.fang@newcastle.edu.au (C. Fang).

https://doi.org/10.1016/j.envpol.2022.118857
Received 6 October 2021; Received in revised form 28 December 2021; Accepted 12 January 2022
Available online 13 January 2022

along with nanoplastics potentially (Efimova et al., 2018). However, we do not know too much about this process due to the absence of the effective characterisation of microplastics and nanoplastics (Ivleva, 2021).

Raman spectroscopy is emerging technique for the characterisation of microplastics (Araujo et al., 2018) and nanoplastics (Fang et al., 2020), via analysis of their unique Raman 'spectral fingerprint'. Raman imaging combines Raman spectroscopy with microscopy and works by scanning a defined area of the sample surface point by point. By collecting the Raman spectrum from the point array as a spectrum matrix, Raman imaging can map the Raman intensity at each point as a pixel, to generate an image. As a result, the signal-noise ratio is increased from this spectrum matrix as compared with that from an individual spectrum (Fang et al., 2020). This means Raman imaging has the potential to analyse weak Raman signals in the presence of background interferences (e.g. plastic additives) (Lenz et al., 2015). The signal-noise ratio of Raman imaging can be further enhanced using effective algorithms to process the spectrum matrix and images (Fang et al., 2021b). Despite its effectiveness, optimisation and validation of this Raman imaging are still needed before the standardised protocols can be developed.

This study aims to demonstrate the application of Raman imaging to identify microplastics and nanoplastics generated when a PVC pipe is cut using different saws. Raman imaging aided with logic-based algorithm is applied to characterise both the PVC microplastics detached from the saws and the nanoplastics bound to the surface of the saw blades. We also discuss the technical challenges associated with the Raman imaging, such as the selection of the focusing plane and the objective lens with different magnifications. The results will potentially form an important part of our method validation process, particularly towards the characterisation of nanoplastics. It is also expected that this study's findings will assist in justifying the need for further research into the microplastics and nanoplastics generated in our daily life, as a way to raise public awareness and better inform policymakers to seek approaches to minimise microplastic and nanoplastics contamination.

2. Materials and methods

2.1. Samples

All PVC pipes and saws were purchased from a local store (Bunnings Warehouse, Australia). An aluminium tray was also purchased from the same store. The saw blades and pipes were cleaned using tap water. The saw blades were further cleaned with acetone, to remove the protective oil on the surface.

We cut the PVC pipes in a backyard garden using different saws, including two hand saws and a jigsaw, along the cross-section direction as shown in Figure S1 (Supporting Information). We observed differences in the size and amount of PVC particles generated when we used different saws to cut the different pipes. In this study, we focused our test on the hand saw (30 cm × 10 cm × 0.1 cm) to cut a PVC pipe with a diameter of 75 mm, which is commonly encountered in our gardens.

During the cutting process, an aluminium tray was positioned on the ground to collect the cutting particles. After cutting, the hand saw was patted vigorously, in order to dislodge the large particles from the saw blade surface down to the aluminium tray. These particles were transported on the glass slide surface for the Raman test, or onto an A4 paper surface, to take a photo towards counting the number of particles, using software ImageJ (Figure S1, Supporting Information).

Using an angle grinder, the saw blade was cut into small pieces of ~5 cm × ~5 cm, for the Raman test and to record a photo image (Figure S2, Supporting Information). For scanning electron microscopy (SEM) and the energy-dispersive X-ray spectroscopy (EDS) test (Figure S3, Supporting Information), a small blade piece was sputter-coated with a thin layer of platinum (~6 nm).

2.2. Raman

Raman spectra were recorded in air using a WITec confocal Raman microscope (Alpha 300RS, Germany) equipped with a 532 nm laser diode (<30 mW), as reported before (Fang et al., 2020; Sobhani et al., 2019; Sobhani et al., 2020). In general, a CCD detector was cooled down to −60 °C and used to collect Stokes Raman signals at room temperature (~24 °C), under the objective lens with magnifications of 20 × , 40 × or 100 × . Their numerical apertures (*NA*) are 0.4, 0.6 and 0.9, respectively.

To map the image, the Raman signal was collected at a general point/pixel size of 2.7 μm × 2.7 (or as indicated later) when the laser was scanning the sample surface. The pixel size, such as at 2.7 μm × 2.7 μm, was controlled by selecting the scanning area (e.g., 80 μm × 80 μm) and adjusting the scanning pixel array (e.g., 30 × 30). The different plastics exhibit different Raman activity and emit different intensities of Raman spectra, as suggested before (Sobhani et al., 2019). For example, the Raman signal at 2910 cm^{-1} was picked up to image the PVC, along with other characteristic peaks (620 cm^{-1}, 690 cm^{-1}, 1330 cm^{-1}, 1430 cm^{-1}). The intensities at different peaks with the selected peak width were mapped as images.

The collected Raman signal was analysed using WITec Project software. By just picking up the net intensity of their unique/characteristic peaks for image mapping, the interference which might originate from the background noise (such as fluorescence), or organic matter, can be effectively avoided by subtracting the baseline of the collected Raman spectra to get the net intensity (the peak area or sum, after automatic integration via software) at the selected peaks. That is, the background has been intentionally subtracted using the collected signal at both sides of the selected Raman peak at the pixels as the background. To further avoid the "bias and false" imaging, an imaging-algorithm analysis is recommended.

2.3. Image analysis: logic-based algorithm

From the Raman spectra matrix, several images were simultaneously mapped at different peaks, such as for PVC at 620 cm^{-1}, 690 cm^{-1}, 1330 cm^{-1}, 1430 cm^{-1}, and 2910 cm^{-1}. At these peak positions, the intensity signal can be mapped as different colours of images. Two or more images, which correspond to two or more different characteristic peaks, can be merged, by logic-OR. In this case, any mapped signal and noise (at each pixel or point) from any image (parent images) will be picked up and merged into a new image (daughter image).

For the algorithm analysis, we employed the ImageJ software. In general, the parent Raman images are opened by the software and processed and merged with a calculator of logic-OR. Another option is conducted by colour-channel-merging.

2.4. SEM and EDS

An SEM (Zeiss Sigma VP) equipped with a backscattered electron detector (BSD) was used to characterise the morphology of the microplastics and nanoplastics, in addition to EDS detection (Octane Pro A).

3. Results and discussion

3.1. Photo images, typical histograms and SEM images

Figure S1 (Supporting Information) shows the saws and the PVC pipes that we tested in this study. During the cutting process, no matter what kind of saw (we tested three) and PVC pipes (we tested two) were used, the released particles could be observed by the naked eye. The typical and representative particles we collected are shown in Fig. 1(a). Due to the resolution limit of the camera that used to take the photo, these particles are generally estimated at sizes bigger than 0.1 mm. Whilst the exact size and quantity of these particles depend on the

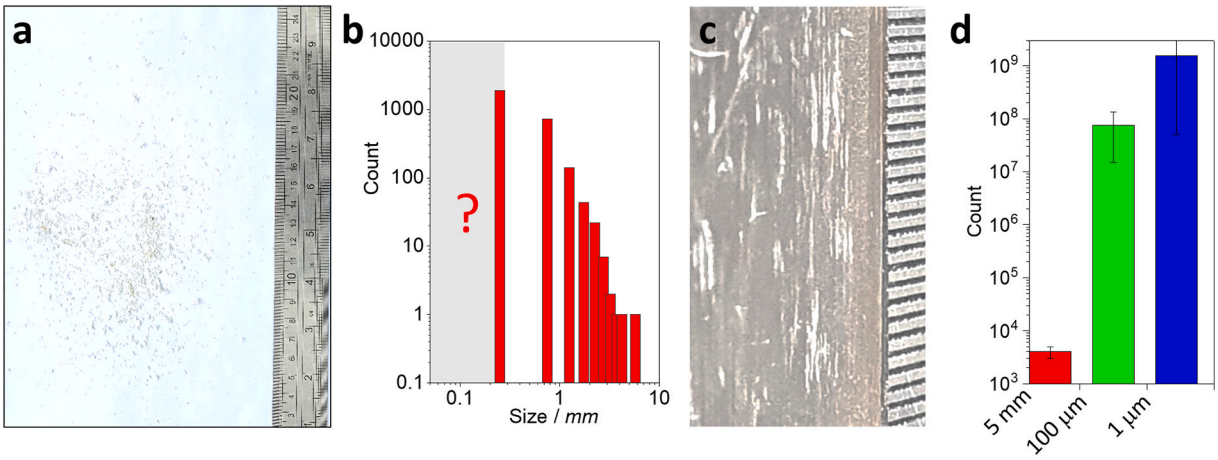

Fig. 1. Photo images (a, c) and histograms (b, d) of the released particles when cutting a PVC pipe. (a) shows the typical particles fallen down and collected in a tray during a cutting process. (b) is the size histogram of the large particles (>0.1 mm) collected in (a). (c) shows that there are lots of small particles sticking on the saw blade surface. The minimum scale in the rule in (c) is 0.5 mm. (d) is another histogram of the particles presented in (a, c).

cutting saw, cutting habits/skills, and pipe materials, the typical results are similar, and the representative histogram analysis of particle size is shown in Fig. 1(b)/S1 (Supporting Information). Since the pipe is mainly made of PVC, the particles may be linked to PVC microplastics, although the scientific proof is needed, and this is provided in the following sections.

In Figs. 1(b), 3000–5000 particles were collected and counted. However, the small ones are not included here, and their amount might be significantly larger than the larger particles, as marked in Fig. 1(b) (the question mark). These small particles could either fall into the aluminium tray (Figure S1, Supporting Information), or stick onto the saw blade surface, as presented in Fig. 1(c). To simplify the sample preparation in our test, we will focus on the particles attached to the saw blade surface. Similarly, using ImageJ software to analyse the photographs taken by the microscopy in Figure S2 (Supporting Information), we can estimate the number of these small particles and categorise them by size, as shown in Fig. 1(d). This technique recorded a significant number of tiny particles.

Fig. 2 shows the SEM images of the particles and films sticking on the saw blade surface. In (a), it can be seen that the PVC particles can be generated on the saw tooth. In the meantime, a significant number of particles remain on the saw blade surface, as presented in Fig. 2(b and c). The particles are typically <100 µm, as the bigger particles tend to fall onto the aluminium tray, as shown in Fig. 1(a)/S1 (Supporting Information). Depending on the cutting techniques, operating conditions and duration, a PVC film might be formed on the saw surface, as presented in Fig. 2(d). Beyond the particles (1–100 µm) in Fig. 2(b, c, e) and the film (d), tiny particles of <1 µm can be observed in Fig. 2(f), which can be categorised to nanoplastics (Gigault et al., 2021; Schwaferts et al., 2020; Sun et al., 2020), if released from the PVC material.

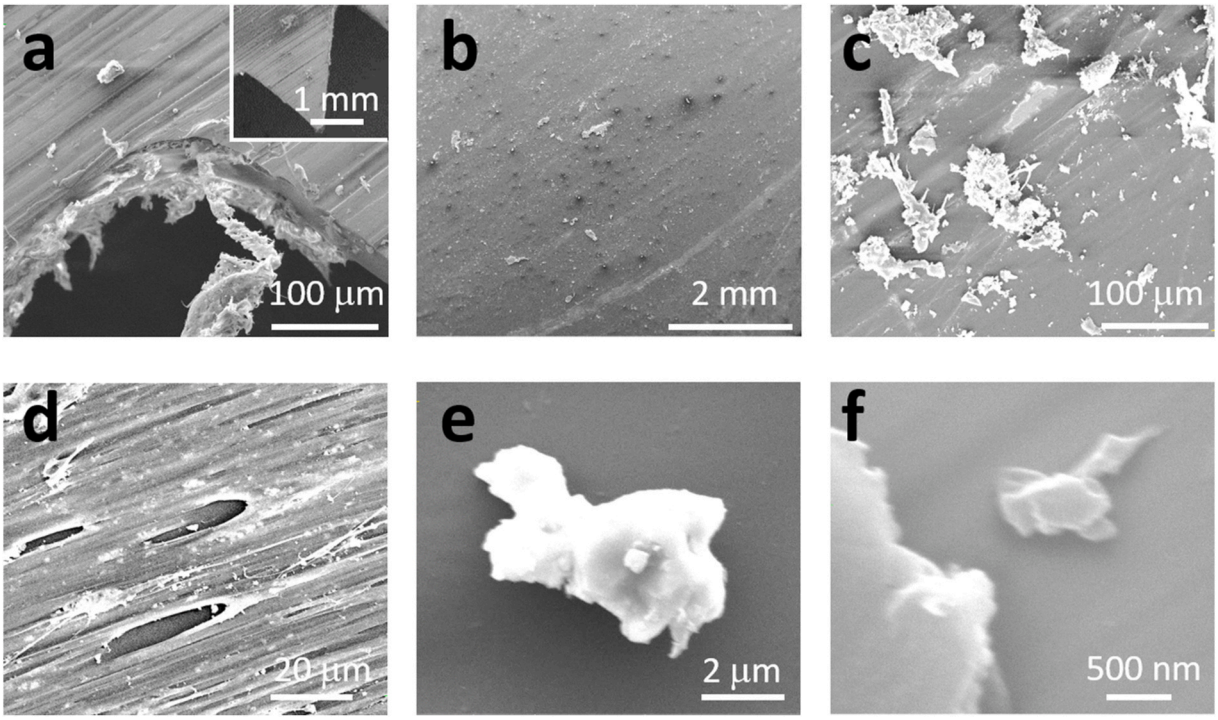

Fig. 2. SEM images of the PVC particles sticking on the saw surface. (a) shows the particles around the saw tooth. (b, c) show the particles under different magnifications. (d) presents a film formed on the saw blade surface. (e, f) show the typical particles at a small size.

As mentioned above, we can assume these particles are PVC microplastics or nanoplastics. EDS measurements provide preliminary confirmation of the presence of PVC, due to the appearance of chlorine that is specific for the PVC plastics, as indicated by the EDS spectra in Figure S3 (Supporting Information). In the following sections, we employ the molecular spectrum of Raman to identify and confirm our assumption (Koelmans et al., 2019; Picó and Barceló, 2019). We test the big particles collected in the aluminium tray first, then the film and the small particles sticking to the blade surface.

3.2. Microplastics collected by the aluminium tray

When scanning the surface of the particles collected in the aluminium tray, the individual Raman spectra in Fig. 3(a) were collected, including 3 spectra with a relative high signal-noise ratio (#1), a middle one (#2), and a low one (#3) (as the spectrum background). From the individual spectrum, it is difficult to identify whether the particles in Fig. 3(b) are plastic or not, and this identification might lead to a "false" positive/negative analysis on the microplastics. However, for images mapped from the scanning spectrum matrix that contain 900 (30 × 30) sets of spectra, the signal-noise ratio is considerably higher than that from a single spectrum, from a statistical point of view (Sobhani et al., 2019). In other words, the image analysis of the microplastics yields a much higher certainty than the spectrum analysis. The results are shown in Fig. 3(c–q).

In Fig. 3(b), there are two neighbouring particles. Their sizes are different, along *x*-*y*-*z*-axis. While the position on a *x*-*y*-plane can be controlled by the scanning stage, the *z*-coordinate is adjusted by focusing. In Fig. 3(c–m), the top row (c-g) shows the results collected when the laser was focused on the top particle in (b), while the middle row (i-m) focused on the bottom particle in (b). Between these two planes of focus, a distance along the *z*-axis of approximately 50 μm has been physically adjusted. That is, at the same *x*-*y*-coordinates, we scanned twice at different positions of the *z*-axis and generated two Raman spectrum matrices, to map the characteristic peaks of PVC. Consequently, from these images (c-m), we can see the patterns matched with the squared two particles in Fig. 3(b), even though there was some blurring of the images. Specifically, the top particle in 3(b) can be visualised in Fig. 3(c–g), while the bottom particle in 3 (b) can be visualised in (i-m). The formation of the blurred image is because, although the pipe is mainly made of PVC, some additives in the pipe material can complicate the Raman analysis, such as by yielding the fluorescence background, as shown in Fig. 3(a) (and supported by EDS in Figure S3, Supporting Information). Also in Fig. 3(a), the different peaks of PVC yield different intensities intrinsically, which leads to the different brightness of mapping images, with some being clear and some others blurred (Fang et al., 2021a).

In Fig. 3, by comparing the top row (c-g) with the middle row (i-m), we can see the effect of the focus of the confocal Raman, when changing the focusing position along the *z*-axis. That is because the sizes of the two particles in Fig. 3(b) are different, particularly along the *z*-axis direction, so we need to change the focusing plane to scan twice. To simultaneously visualise the two particles, we can merge the information collected from those two scans, such as by merging the images in Fig. 3 (g, m) (mapped at the strong peak of 2910 cm^{-1}), to generate a daughter image in (n). The image in Fig. 3(o) with a clean background (white) and contour lines can provide another version of observation, in order to visualise their distribution. We even can overlay the daughter image (n) on the photo image to generate another image of Fig. 3(h) (with emphasis on the outline of the particle profile). The well-matched pattern suggests the success of the Raman imaging. Based on this test, most of the particles in Fig. 1(a and b) can be assigned to the PVC microplastics.

The different focusing position along the *z*-axis can be presented in Fig. 3(p, q), via the 3D presentations (Sobhani et al., 2019), with a physical distance of ~50 μm. Note that the two merged images are

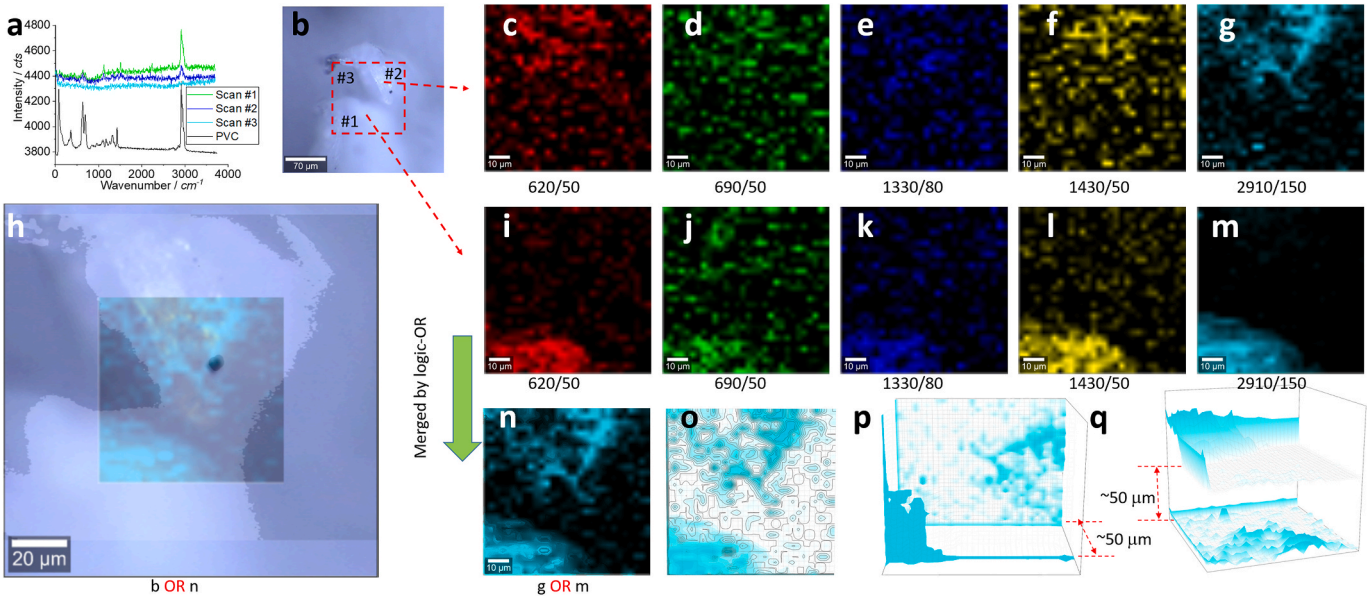

Fig. 3. Typical Raman spectrum (a), photo image (b) and Raman intensity images (c–q) of two particles collected in the tray. In (a), the standard spectrum of PVC is presented to compare with 3 typical spectra collected (positions marked in (b)) during the scanning process, including a relatively strong one (#1), a medium one (#2) and a weak one (#3) collected from the blank area as the spectrum background. The squared area of 80 μm × 80 μm in (b) was scanned twice with a different focusing plane and all Raman spectra were collected at an objective lens of 20 × , with a pixel of 2.7 μm × 2.7 μm (to generate two spectrum matrices of 30 × 30) and 1 s integration. (c–g) were mapped when the laser was focused on the top particle in (b), while (i–m) focused on the bottom particle. The distance between the two focusing planes along the *z*-axis is ~50 μm. The intensity images (c–m) are mapped at the characteristic peaks of PVC (620 cm^{-1}, 690 cm^{-1}, 1330 cm^{-1}, 1430 cm^{-1} and 2910 cm^{-1}), as marked under the images (and the peak width), with background correction and 10% colour off-setting. The numbers below Raman images, for example, 620/50 indicates the integration of peak intensity between 595 cm^{-1} (620–50/2) and 645 cm^{-1} (620 + 50/2). (n) is a merged image of (g, m), using logic-OR. (o–q) are other versions of (n), with white background (o) or using 3D presentation (p, q). (h) is a merged image of (b, n). (For interpretation of the references to colour in this figure legend, the reader is referred to the Web version of this article.)

mapped as Raman intensity, which is not directly related with the physical size or position along the *z*-axis. In other words, the confocal Raman has a disadvantage and cannot simultaneously (via one Raman scanning) characterise microplastics of different sizes (particularly along *z*-axia). In this case, we need to categorise the microplastics to different sub-groups, in order to avoid the shielding of small particles by the big particles within one Raman scan, such as if the scan was focused on the big particles, or vice versa. In the following sections, we will test the microplastics in the range of 1–100 μm first, then down to <1 μm.

In Fig. 3(h), we can see that only parts of the two particles have been effectively visualised and identified as PVC, even with two Raman scans. However, we can "expand" the tested/identified parts to the whole particles within the physical boundary or profile outline of the particles, given the particle is made of the same material of PVC uniformly. In this case, we can even simplify the scanning process to just map the physical boundary, intentionally and selectively. By doing so, we can significantly shorten the Raman scanning duration. More research is needed.

3.3. Microplastic film sticking on the saw blade surface

As mentioned above, depending on the cutting conditions, there might be a film formed on the saw blade surface, which is tested in this section, before testing the small particles in the following sections.

The film can be easily broken, as observed in Fig. 2(d)/4(a). When mapped using Raman imaging, an image in Fig. 4(b) is generated. Herewith only the strong peak at 2910 cm^{-1} is mapped to simplify the analysis. The boundary between the film and the empty/broken area is effectively mapped in Fig. 4(b) as a horizon line, which is due to the confocal setup again (Sobhani et al., 2019). That is, the uneven surface of the saw blade means only the focused position can be effectively imaged, which is on the boundary of the broken film. The weak signal from the unfocused position is mapped as the image background in Fig. 4 (b), along with noise.

When zoomed in using a higher magnification of lens (40 × *vs.* 20 ×), the images in Fig. 4(c and d) are produced. Basically, similar results are obtained, the horizon boundary of the broken film is effectively displayed again. Similar results are achieved in Fig. 4(e and f), when further zooming in using a magnification of lens of 100 × . When a small area was scanned to generate an image with a higher resolution or a smaller pixel size (0.33 μm × 0.33 μm in (g) *vs.* 1 μm × 1 μm in (f) *vs.* 2.7 μm × 2.7 μm in (b, d)), the image in Fig. 4(g) is mapped along the horizon boundary again. It can be overlaid onto the photo image to generate the image in Fig. 4(h). The well-matched pattern demonstrates the effectiveness of the Raman imaging in visualising PVC plastics. From this test, we can link most of the films in Fig. 1(c and d)/2(d)/S2(a, c) to PVC.

In Fig. 1(c)/2(d)/4, the film surface area varies from several μm^2 to mm^2, with a thickness of <2 μm (measured by tilting the SEM sampling holder to gain a side view). In Fig. 2(d), we can see that the film is an aggregate of particles and shreds, which might be another possible reason that results in the blurred patterns in Fig. 4. In the following section, we will test the individual particles adhering to the saw blade surface, in order to obtain a clearer pattern.

3.4. Microplastic particles sticking on the saw blade surface

We tested the small particles sticking on the saw blade surface in the range of 1–100 μm and the typical results are shown in Fig. 5. Under the optical microscope, the images in Fig. 5(a and b) can visualise the particles, and most of them are in the range of 1–100 μm. We selected a small "black" particle for the Raman test and the results are presented in Fig. 5(c–i).

Again, in Fig. 5(c), from the Raman spectra including a relatively strong one (#1), a middle one (#2) and a weak one (#3), it is difficult to justify the presence of PVC due to the low signal-noise ratio, particularly due to the high spectrum background of fluorescence. Fortunately, the images in Fig. 5(d–i) that were mapped at the characteristic peaks of PVC can generate the clear pattern that matches well with that in Fig. 5 (b), suggesting the presence of PVC. The reason has been discussed, which is that mapping from the spectrum matrix that contains 1600 (40 × 40) sets of Raman spectra can increase the signal-noise ratio. The background in Fig. 5(b), the horizon line, is not mapped, indicating it is not PVC, but the uneven surface of the saw blade.

To further improve the signal-noise ratio and the imaging certainty, we can merge the images together and get the image in Fig. 5(d), using logic-OR. The bright area (spot) contains all the contributions from the characteristic peaks of PVC, and thus can further confirm the presence of PVC. Some red background (the image background, not the spectrum background) is due to the low peak intensity of PVC at 620 cm^{-1}, as discussed above. However, the low signal-noise ratio in Fig. 5(e) is increased in Fig. 5(d), using a logic-based algorithm.

Herewith we map the Raman intensity at the characteristic peaks or

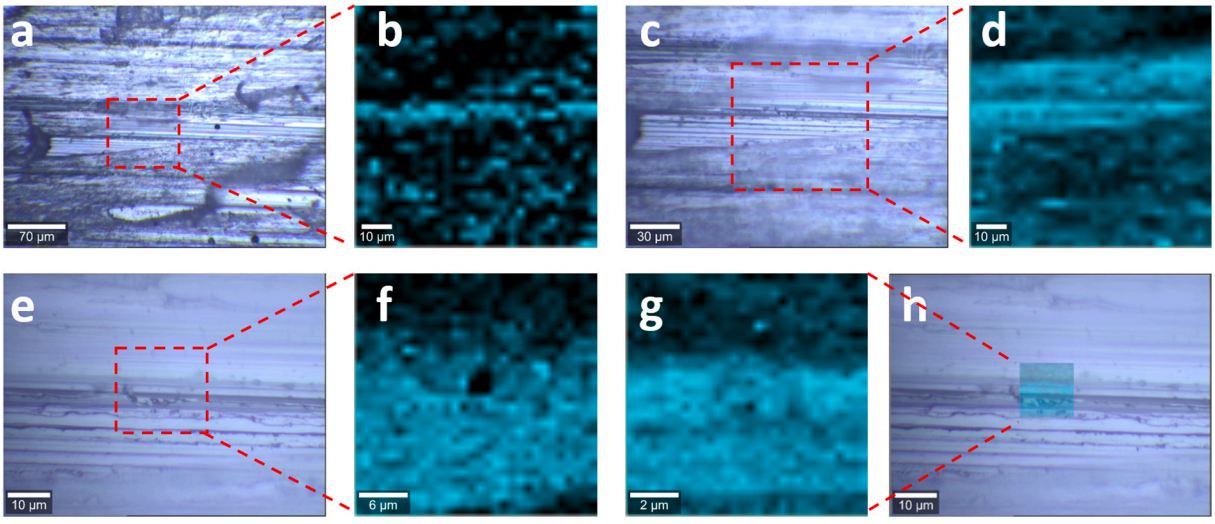

Fig. 4. Photo images (a, c, e, h) and Raman intensity images (b, d, f-h) of a film sticking on the saw blade surface. The scanning areas are squared in (a, c, e) and Raman intensity images (b, d, f, g) are mapped at peak 2910 cm^{-1} when scanned using difference magnifications of the lens of 20 × (a, b), 40 × (c, d) and 100 × (e–h). (h) is an image of (g) overlapped on (e). All Raman intensity images are corrected with background and 10% colour off-setting, from the Raman spectrum matrix of 30 × 30. (For interpretation of the references to colour in this figure legend, the reader is referred to the Web version of this article.)

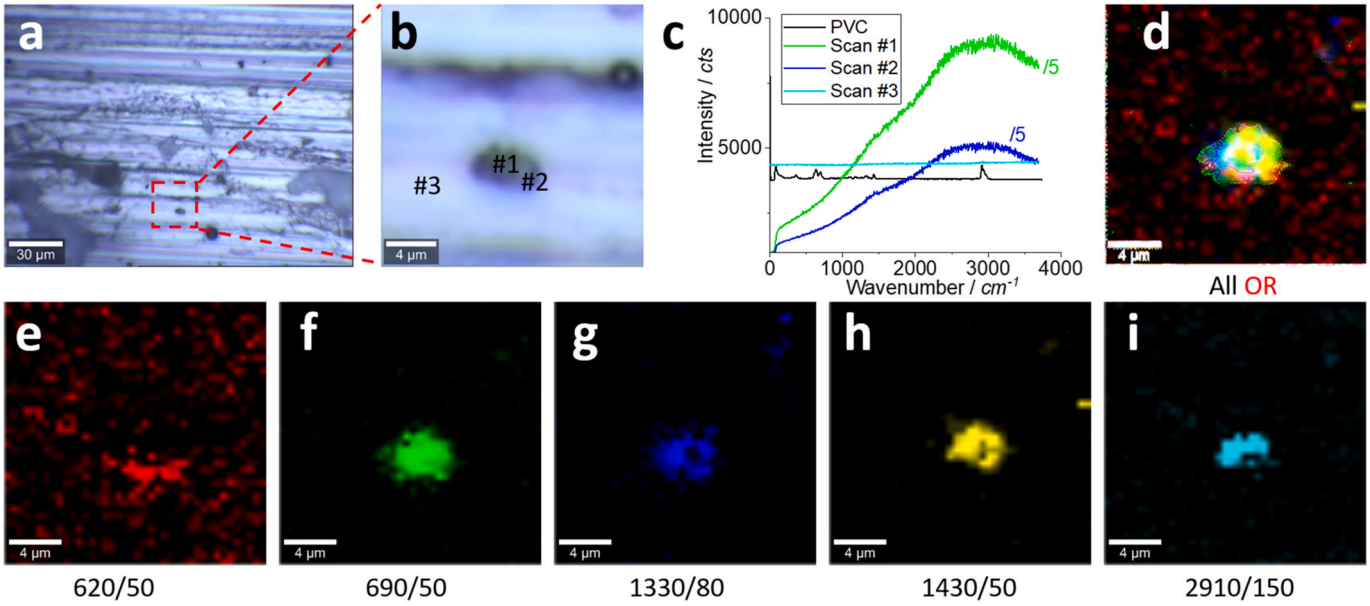

Fig. 5. Photo images (a, b), typical Raman spectrum (c) and intensity images (d–i) of a small particle sticking on the saw blade surface. The squared area of 20 μm × 20 μm in (a) was scanned and all Raman spectra were collected (positions marked in (b)) at an objective lens of 40 × , with a pixel of 0.5 μm × 0.5 μm (to generate a spectrum matrix of 40 × 40) and 1 s integration. (c) shows the standard spectrum of PVC to compare with 3 typical Raman spectra collected during the scanning process (#1–2's intensity has been divided by 5, while #3 as the spectrum background). The intensity images (e–i) are mapped at the characteristic peaks of PVC (620 cm^{-1}, 690 cm^{-1}, 1330 cm^{-1}, 1430 cm^{-1} and 2910 cm^{-1}), as marked under the images (and the peak width), with background correction and 10% colour offsetting. (d) is a merged image of (e–i), using logic-OR. (For interpretation of the references to colour in this figure legend, the reader is referred to the Web version of this article.)

wavenumber windows of PVC. If we map the non-characteristic windows where the PVC does not emit the Raman signal, the images are generated and shown in Figure S4. Basically, if there is no contribution from the PVC plastic, only noise is mapped and no clear pattern is produced, which can further confirm the assignment of the mapped pattern in Fig. 5 as a PVC microplastic.

3.5. Effect of the objective lens with different magnifications

Although we successfully detected PVC microplastic of ~3 μm in Fig. 5, it is difficult to go further down to capture nanoplastics directly. That is because (i) the scanning duration can be extremely long. In Fig. 5, using a pixel of 0.5 μm × 0.5 μm with an integration time of 1 s, it took 1600 s (40 × 40) to scan an area of 20 μm × 20 μm. It will take as long as 25,600 s (~7.1 h) to scan an area of 80 μm × 80 μm; (ii) Even so, the pixel size of 0.5 μm × 0.5 μm means that the smaller particles (<0.5 μm × 0.5 μm) cannot be clearly visualised in the *x*-*y*-plane; (iii) in the *z*-axis direction under the confocal Raman, nanoplastics mixed with microplastics can be easily shielded, shadowed and hidden by the large ones, as suggested by the results in Fig. 3. We usually map the particles over a large area using a large pixel size under an objective lens of 20 × . We then gradually narrow down to a smaller area using a smaller size of pixel under an objective lens of 40 × , then 100 × , to capture nanoplastics eventually. The change of the objective lens magnification has a significant impact on the results, as shown in Fig. 4, and is further tested in this section. Note, each time when the objective lens is changed, the *x*-*y*-axis position might be shifted slightly, and the *z*-axis position has been changed correspondingly, by re-focusing the laser to maximise the Raman signal.

The images in Fig. 6(a–c) were collected and mapped under a lens of 20 × . We can easily capture and visualise a large particle (~10 μm × ~30 μm) from the Raman images in (b, c). Here the image in Fig. 6(b) is mapped at the strong peak of PVC at 2910 cm^{-1}, the other characteristic peaks are also mapped and merged to one in Fig. 6(c). We can thus confirm the presence of the PVC microplastic. The horizon lines in (a) are not mapped in (b, c) again and are assigned to the bumpy surface of the saw blade, originating from the fabrication process.

However, the fine particles are neither clearly observed nor effectively patterned under this lens. When zoomed in using a lens of 40 × , the image in Fig. 6(d) shows several small particles in the size range of 3 μm–20 μm on the top area of the large one mapped in Fig. 6(b). Once mapped using Raman, the images in Fig. 6(e and f) are generated. Similarly, the clear pattern in (e) is due to the strong peak at 2910 cm^{-1}, while the blurred pattern in (f) can be attributed to the weak peaks. Again, we can assign them to the PVC microplastics, although they have not been well mapped in Fig. 6(b and c), akin to being hidden in the shadow of the large one. The changed lens with a higher *NA* (0.6 *vs.* 0.4) leads to a more effective collection on the Raman signal.

Once zoomed in again using a lens of 100 × (with an *NA* of 0.9), the images in Fig. 6(g–i) are obtained. More fine particles can be mapped and visualised in the size range <5 μm. Due to the reduced size, the Raman signal has weakened, and the image in Fig. 6(i) hardly shows the pattern outline that agrees with that in Fig. 6(g and h).

Even though we used a lens of 100 × , and the image pixel was improved to 1 μm × 1 μm, the images in Fig. 6(g and h) might still not be able to display some fine particles, such as nanoplastics. In the following section, we further scan and detail the area squared in Fig. 6(h).

3.6. Nanoplastics sticking on the saw blade surface

Fig. 7 shows the test results when the pixel was further decreased from 1 μm × 1 μm–0.33 μm × 0.33 μm. Also, the integration time at each pixel was prolonged from 1 s to 2 s. By doing so, we try to capture nanoplastics which emit the weak Raman signals.

Fig. 7(a) marks the positions where the Raman spectra were collected. The spectra are shown in Fig. 7(b). Compared to Fig. 5(c), the signal-noise ratio of the spectrum has been improved. However, it is still difficult to justify the PVC plastics from the single spectrum and we use Raman imaging again. The peak at 2910 cm^{-1} is relatively strong so we mapped its intensity and generated images in (c, d). Several nanoplastics were effectively mapped, which can be obviously observed in (d), via the 3D presentation. Some nanoplastics cannot be observed in Fig. 7(a),

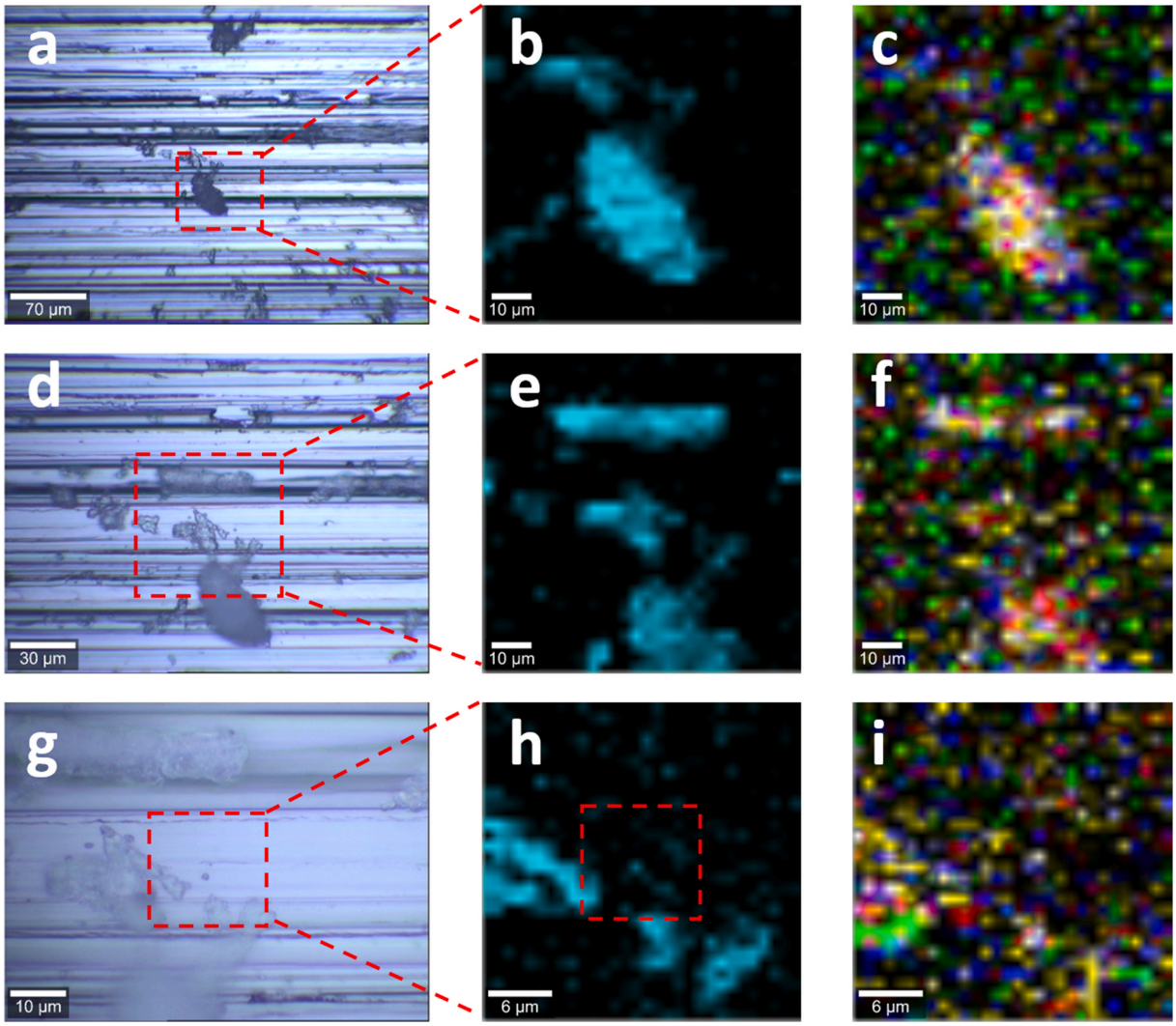

Fig. 6. Photo images (a, d, g), and Raman intensity images (all the rest) of the PVC particles sticking on the saw blade surface. The squared areas in (a, d, g) were scanned under different magnifications of lens of 20 × (top row), 40 × (middle row) and 100 × (bottom row). Raman spectra were collected with a pixel of 2.7 μm × 2.7 μm for the top and middle rows, or 1 μm × 1 μm for the bottom row, and 1 s integration for each pixel. The intensity images are mapped at the characteristic peak of 2910 cm^{-1} in (b, e, h), or at other peaks but merged in (c, f, i), with background correction and 10% colour off-setting, from the Raman spectrum matrices of 30 × 30, using logic-OR. The squared area in (h) is further tested in Fig. 7. (For interpretation of the references to colour in this figure legend, the reader is referred to the Web version of this article.)

under the optical microscope, highlighting the advantage of Raman imaging. However, given the diffraction of the laser spot (focused as an Airy or Fresnel disk, and resulted in an image resolution at $\sim\lambda/2NA$. For a laser wavelength λ of 532 nm, it is ~300 nm when *NA* is 0.9 for a 100 × lens), the small ones (<300 nm) should be cautiously justified as nanoplastics (Fang et al., 2020).

To further confirm above assignment, in Fig. 7(e), we show the mapped image without the spectrum background correction. Here the colour scale bars are also presented to see the intensity change. Compared (e) with (c, d), the similar patterns are generated. However, the intensity in (e) is much higher than that in (c, d) (the maximum of 241,200 cts *vs.* 2203 cts, presented by the colour scale bar), suggesting the mapped signal is dominated by the spectrum background. Even so, the colour off-setting in (e) still enables the visualisation of the PVC plastic.

In Fig. 3(a)/7(b), in some wavenumber areas or windows, the PVC plastic does not emit the characteristic Raman signal, such as at 2550 cm^{-1} and 3500 cm^{-1}. Within those wavenumber windows, the Raman intensities can also be mapped as images, which act as the "internal reference" or "blank" to check the background, as presented in Fig. 7(f and g). Once the spectrum background is corrected, however, only noise is mapped in (f, g), because of the absence of the PVC contribution. In other words, if there is no PVC plastic, there is no clear pattern, which can confirm the assignment of the pattern in Fig. 7(c–e) as PVC microplastics or nanoplastics.

These test can lead us to assign most of the particles in Fig. 1(b and c)/S2(b, d) to the PVC microplastics and nanoplastics, echoing the SEM images in Fig. 2. However, while the advantages of the Raman imaging are appreciated, we should also keep in mind the disadvantages, including (i) the confocal setup is constrained by the focus issue which prevents simultaneous mapping microplastics of different sizes and at the different positions along the *z*-axis (i.e., they are not localised on the same focus plane), as demonstrated in Fig. 3. Consequently, we recommend that microplastics are categorised into different size groups, for Raman imaging; (ii) Whist Raman imaging might be time consuming, the process can be improved by selectively mapping the microplastics boundary, rather than mapping the whole area, if the microplastic is large and the boundary is available; (iii) different magnifications of lens with different *NA* can affect the mapping results, as shown in Fig. 4. Therefore, the small particles, if mixed with the big ones, can be shielded

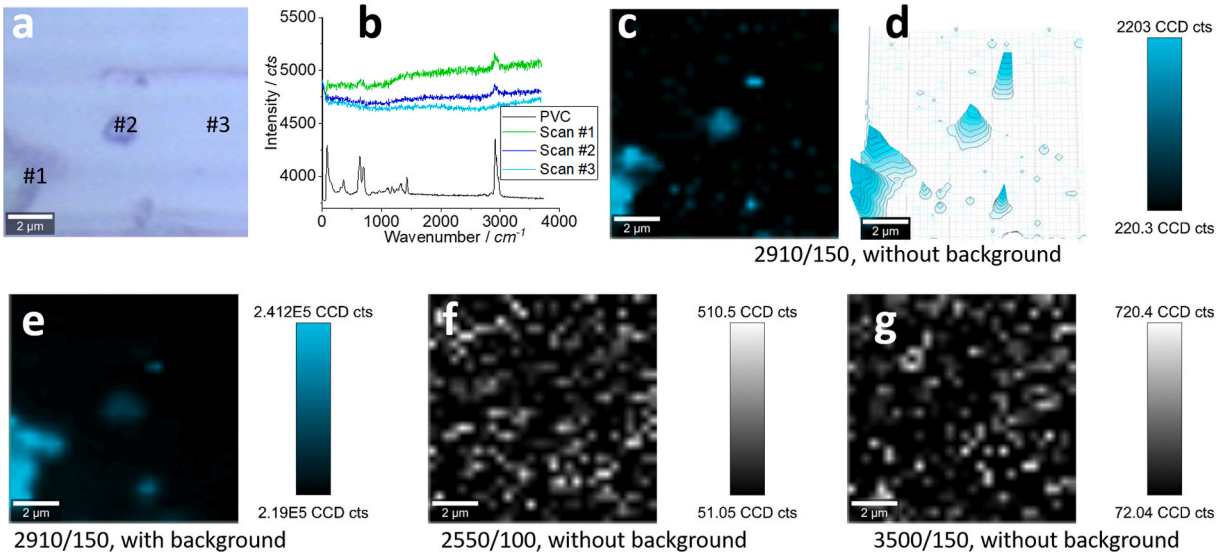

Fig. 7. Photo image (a), Raman spectra (b) and Raman intensity images (c–g) of the PVC particles sticking on the saw blade surface. (a) marks the collection positions for spectra in (b) to compare with a standard Raman spectrum of PVC, including a relatively strong one (#1), a medium one (#2) and a weak one (#3) collected from the blank area as the spectrum background. The area in (a) was squared in Fig. 6(h) and scanned under a lens of magnification 100 × . All Raman spectra were collected with a pixel of 0.33 μm × 0.33 μm (to generate a spectrum matrix of 30 × 30), and 2 s integration for each pixel. The intensity image (c) is mapped at the characteristic peaks of 2910 cm^{-1}, with background correction and 10% colour off-setting. (d) is another version of (c), using a 3D presentation. (e) is also another version of (c), but without spectrum background correction. (f, g) are mapped at non-characteristic wavenumber windows of PVC, with spectrum background correction and with 10% colour off-setting, as the internal reference to show the image background. The colour scale bars are presented for the Raman intensity images. (For interpretation of the references to colour in this figure legend, the reader is referred to the Web version of this article.)

and cannot be mapped, as shown in Fig. 6; (iv) when the mapping pixel is decreased and the integration time is increased in order to capture nanoplastics, the scanning duration is prolonged further. We thus recommend a gradual zooming-in approach, within the plane of the *x*-*y*-axis, to get the detailed/fine particles/structures, as shown in Figs. 6–7. Even so, as mentioned above, due to the laser diffraction (resulting in the imaging resolution at $\sim\lambda/2NA$ of ~300 nm) and the scanning pixel size (330 nm × 330 nm in Fig. 7) (Fang et al., 2020), small nanoplastics (<300 nm) are still faced with the visualisation challenge via Raman imaging.

One possible approach to visualise nanoplastics is scanning near-field optical microscopy (SNOM). By focusing the excitation laser through an aperture with a diameter smaller than the laser wavelength, SNOM can extend the spatial resolution into the nanometre range (Kohli, 2012; Zhang et al., 2017). Another approach to break through the laser diffraction limit is the newly developed super-resolution imaging, such as photo-activated localisation microscopy (PALM) and stochastic optical reconstruction microscopy (STORM) (Kamiyama and Huang, 2012; Zanacchi and Diaspro, 2013). Unlike the confocal Raman microscopy employed here, PALM/STORM are wide-field imaging techniques via fluorescence microscopy (no need to scan) to quickly obtain images with the image resolution even down to a few nanometres or a single molecule. For the confocal Raman imaging employed here, to visualise nanoplastics, we can also further decrease the scanning pixel size, such as down to 40 nm × 40 nm, and select a suitable colour off-setting (Fang et al., 2020). This is because, for a laser to scan an individual nanoplastic (smaller than the laser spot size) with a decreased pixel size (also smaller than the laser spot size), the collected Raman intensity (at the characteristic peaks) from the scanning spectrum matrix behaves a lateral Gaussian distribution. The subsequent colour off-setting helps to identify the central position of the Gaussian distribution towards the visualisation and localisation of nanoplastic. Compared to the wide-field imaging PALM/STORM, the scanning duration of the confocal Raman imaging is much longer, particularly when the scanning pixel size is further decreased. The weak Raman signal can also easily leads to false positive/negative characterisation of nanoplastics. More research is needed to explore their applications for nanoplastics analysis.

4. Conclusion

We demonstrated how to capture microplastics and nanoplastics via Raman imaging. The advantages and disadvantages of this characterisation approach have been carefully compared and balanced. Overall, we have concluded that this approach is effective to characterise the microplastics and particularly nanoplastics, and have provided some suggestions and recommendations to consider in applying the Raman imaging technique.

We validated this approach to capture the microplastics and nanoplastics released when we cut PVC pipe in our gardens. Depending on the cutting conditions, thousands of microplastics might be released from each cutting process, which can be easily observed by the naked eye. Regarding those “invisible” nanoplastics, we estimate that billions of them are likely generated.

To address the concerns of the microplastics contamination, we are expanding this Raman imaging approach to identify more sources that might create microplastics and nanoplastics, which will be reported soon.

Credit authors statement

Cheng Fang, Ravi Naidu, were involved experiment design and management. Cheng Fang, Md. Al Amin, Christopher T. Gibson, Clarence Chuah, participated in data collection and sample preparation. Yunlong Luo, Youhong Tang, helped the manuscript preparation and reviewing process.

Declaration of competing interest

The authors declare that they have no known competing financial interests or personal relationships that could have appeared to influence the work reported in this paper.

Acknowledgements

The authors appreciate the funding support from CRC CARE and the University of Newcastle, Australia. For the Raman and SEM measurements, we also acknowledge the use and support of the South Australian node of Microscopy Australia (formerly known as AMMRF) at Flinders University, South Australia.

Appendix A. Supplementary data

Supplementary data to this article can be found online at https://doi.org/10.1016/j.envpol.2022.118857.

References

Araujo, C.F., Nolasco, M.M., Ribeiro, A.M.P., Ribeiro-Claro, P.J.A., 2018. Identification of microplastics using Raman spectroscopy: latest developments and future prospects. Water Res. 142, 426–440.
Barnes, D.K.A., Walters, A., Gonçalves, L., 2010. Macroplastics at sea around Antarctica. Mar. Environ. Res. 70, 250–252.
Boyle, D., Catarino, A.I., Clark, N.J., Henry, T.B., 2020. Polyvinyl chloride (PVC) plastic fragments release Pb additives that are bioavailable in zebrafish. Environ. Pollut. 263, 114422.
Buranyi, S., 2020. The Missing 99%: Why Can't We Find the Vast Majority of Ocean Plastic?.
Efimova, I., Bagaeva, M., Bagaev, A., Kileso, A., Chubarenko, I.P., 2018. Secondary microplastics generation in the sea swash zone with coarse bottom sediments: laboratory experiments. Front. Mar. Sci. 5.
Fang, C., Luo, Y., Zhang, X., Zhang, H., Nolan, A., Naidu, R., 2021a. Identification and visualisation of microplastics via PCA to decode Raman spectrum matrix towards imaging. Chemosphere 286, 131736.
Fang, C., Sobhani, Z., Zhang, X., Gibson, C.T., Tang, Y., Naidu, R., 2020. Identification and visualisation of microplastics/nanoplastics by Raman imaging (ii): smaller than the diffraction limit of laser? Water Res. 183, 116046.
Fang, C., Sobhani, Z., Zhang, X., McCourt, L., Routley, B., Gibson, C.T., Naidu, R., 2021b. Identification and visualisation of microplastics/nanoplastics by Raman imaging (iii): algorithm to cross-check multi-images. Water Res. 194, 116913.
Gigault, J., El Hadri, H., Nguyen, B., Grassl, B., Rowenczyk, L., Tufenkji, N., Feng, S., Wiesner, M., 2021. Nanoplastics are neither microplastics nor engineered nanoparticles. Nat. Nanotechnol. 16, 501–507.
Ivleva, N.P., 2021. Chemical analysis of microplastics and nanoplastics: challenges, advanced methods, and perspectives. Chem. Rev. 121, 11886–11936.
Jamieson, A.J., Malkocs, T., Piertney, S.B., Fujii, T., Zhang, Z., 2017. Bioaccumulation of persistent organic pollutants in the deepest ocean fauna. Nat. Ecol. Evol. 1, 0051.
Kaczorek-Chrobak, K., Fangrat, J., 2020. PVC-based copper electric wires under various fire conditions: toxicity of fire effluents. Materials 13, 1111.
Kamiyama, D., Huang, B., 2012. Development in the STORM. Dev. Cell 23, 1103–1110.
Koelmans, A.A., Mohamed Nor, N.H., Hermsen, E., Kooi, M., Mintenig, S.M., De France, J., 2019. Microplastics in freshwaters and drinking water: critical review and assessment of data quality. Water Res. 155, 410–422.
Kohli, R., 2012. Chapter 5 - developments in imaging and analysis techniques for micro- and nanosize particles and surface features. In: Kohli, R., Mittal, K.L. (Eds.), Developments in Surface Contamination and Cleaning. William Andrew Publishing, Oxford, pp. 215–306.
Lenz, R., Enders, K., Stedmon, C.A., Mackenzie, D.M., Nielsen, T.G., 2015. A critical assessment of visual identification of marine microplastic using Raman spectroscopy for analysis improvement. Mar. Pollut. Bull. 100, 82–91.
Li, L., Luo, Y., Li, R., Zhou, Q., Peijnenburg, W.J.G.M., Yin, N., Yang, J., Tu, C., Zhang, Y., 2020. Effective uptake of submicrometre plastics by crop plants via a crack-entry mode. Nat. Sustain. 3, 929–937.
Naik, R.A., Rowles, L.S., Hossain, A.I., Yen, M., Aldossary, R.M., Apul, O.G., Conkle, J., Saleh, N.B., 2020. Microplastic particle versus fiber generation during photo-transformation in simulated seawater. Sci. Total Environ. 736, 139690.
Napper, I.E., Davies, B.F.R., Clifford, H., Elvin, S., Koldewey, H.J., Mayewski, P.A., Miner, K.R., Potocki, M., Elmore, A.C., Gajurel, A.P., Thompson, R.C., 2020. Reaching new heights in plastic pollution—preliminary findings of microplastics on Mount Everest. One Earth 3, 621–630.
Petersen, F., Hubbart, J.A., 2021. The occurrence and transport of microplastics: the state of the science. Sci. Total Environ. 758, 143936.
Picó, Y., Barceló, D., 2019. Analysis and prevention of microplastics pollution in water: current perspectives and future directions. ACS Omega 4, 6709–6719.
Proshad, R., Kormoker, T., Islam, M.S., Haque, M.A., Rahman, M.M., Mithu, M.M.R., 2018. Toxic effects of plastic on human health and environment: a consequences of health risk assessment in Bangladesh. Int. J. Health 6, 1–5.
Ross, P.S., Chastain, S., Vassilenko, E., Etemadifar, A., Zimmermann, S., Quesnel, S.-A., Eert, J., Solomon, E., Patankar, S., Posacka, A.M., Williams, B., 2021. Pervasive distribution of polyester fibres in the Arctic Ocean is driven by Atlantic inputs. Nat. Commun. 12, 106.
Schwaferts, C., Sogne, V., Welz, R., Meier, F., Klein, T., Niessner, R., Elsner, M., Ivleva, N. P., 2020. Nanoplastic analysis by online coupling of Raman microscopy and field-flow fractionation enabled by optical tweezers. Anal. Chem. 92, 5813–5820.
Sobhani, Z., Al Amin, M., Naidu, R., Megharaj, M., Fang, C., 2019. Identification and visualisation of microplastics by Raman mapping. Anal. Chim. Acta 1077, 191–199.
Sobhani, Z., Zhang, X., Gibson, C., Naidu, R., Mallavarapu, M., Fang, C., 2020. Identification and Visualisation of Microplastics/nanoplastics by Raman Imaging (I): Down to 100 Nm. Water research, p. 115658.
Sun, X.-D., Yuan, X.-Z., Jia, Y., Feng, L.-J., Zhu, F.-P., Dong, S.-S., Liu, J., Kong, X., Tian, H., Duan, J.-L., Ding, Z., Wang, S.-G., Xing, B., 2020. Differentially charged nanoplastics demonstrate distinct accumulation in Arabidopsis thaliana. Nat. Nanotechnol. 15, 755–760.
William Coaker, A., 2003. Fire and flame retardants for PVC. J. Vinyl Addit. Technol. 9, 108–115.
Zanacchi, F.C., Diaspro, A., 2013. Stochastic optical reconstruction microscopy. In: Roberts, G.C.K. (Ed.), Encyclopedia of Biophysics. Springer Berlin Heidelberg, Berlin, Heidelberg, pp. 2475–2476.
Zhang, W., Fang, Z., Zhu, X., 2017. Near-field Raman spectroscopy with aperture tips. Chem. Rev. 117, 5095–5109.